Exploring model-form uncertainties in large-eddy simulations

By S. P. Domino†, L. Jofre AND G. Iaccarino

A variable-density, low-Mach-number turbulent flow validation study has been conducted using the large-eddy simulation (LES) technique. Numerical results are compared to an experimental configuration involving mixed convection heat transfer to a cylinder in cross-flow. The quantity of interest (QoI), heat flux to the cylinder, is compared between the experiment and a variety of LES models. The simulation study outlines a systematic procedure to insure that model-form sensitivities are properly characterized. The methodology includes detailed case identification and validation, formal order-of-accuracy solution verification, and model-form sensitivity studies. Model-form sensitivity for the QoI is based on a variety of LES models: Smagorinsky, wall-adapting local eddy viscosity (WALE), and a one-equation k_{sgs} closure approach. In addition to simple model-form error exploration, injection of uncertainty into the Reynolds stresses through perturbation of the tensor eigenvalues has been extended from Reynolds-averaged Navier-Stokes (RANS) models to the LES subgrid-scale momentum and scalar closure approaches. Simulation studies indicate that the LES technique is far more accurate in predicting heat flux to an object. Model-form sensitivities are also provided in the context of solution verification.

1. Introduction

Sandia National Laboratories continues investment in the prediction of heat flux to objects subjected to the abnormal thermal environment (ATE). The ATE is characterized by a highly sooting hydrocarbon combustion event, whereby an object is heated by both radiative and convective loads. This multi-physics environment is represented by a low-Mach-number reacting flow coupled to both radiation in participating media and the object thermal response. As fire physics understanding has grown, the representative accident scenarios have also changed. Early studies focused on large-scale hydrocarbon outdoor pool fires in quiescent conditions (Gritzo *et al.* 1997). However, experiments have shown that inclusion of cross-flow dramatically augments heat flux to objects due to an increased mixing in the developed counter-rotating vortex (Tieszen 2001). As hydrodynamic mixing increases, the role of accurately predicting convective loads has gained importance. In extreme mixing cases, i.e., fire whirls that can form due to confined scenarios, heat fluxes to an object can increase by a factor of two with respect to quiescent conditions. Therefore, in most recent experimental campaigns that create an ATE, the usage of cross-flow is routine (Hanlin *et al.* 2009).

In support of the ATE validation modeling, an experimental study was conducted to investigate convective heat transfer flux to a cylinder in the presence of imposed shear flow (Kearney *et al.* 2005). The flow channel was capped with a near-adiabatic top wall in addition to a heated or adiabatic bottom wall, while the cylinder was either heated

† Sandia National Laboratories

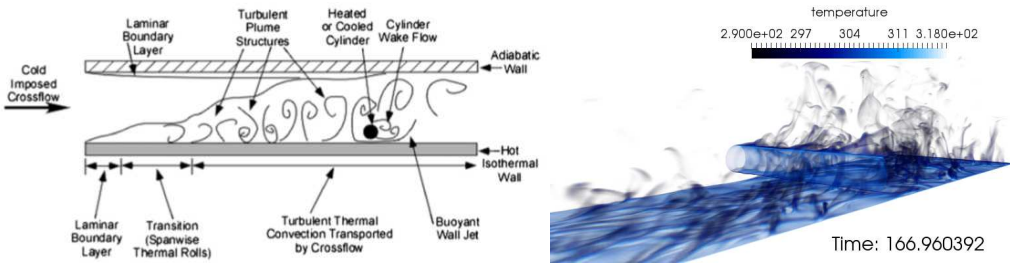

(a) (b)

FIGURE 1. (a) Details of the experimental configuration — figure reproduced from Kearney *et al.* (2005). (b) Representative volume-rendered temperature field from LES simulation with thermal plumes depicted.

or cooled by a high-Reynolds-number (Re = 150k) inner fluid. This flow configuration is depicted in Figure 1(a). The flow is characterized by an incoming laminar boundary layer that transitions due to spanwise thermal plume structures. As the flow proceeds toward the cylinder, a turbulent thermal boundary layer is noted. Although the Reynolds number based on inflow velocity and outer cylinder diameter is low ($Re = 189$), this high-Rayleigh-number flow ($Ra = 10^8$) is challenging to predict due to the presence of thermal plume structures forming, convecting downstream and impinging onto the cylinder. To outline the richness of the problem, a volume-rendered temperature field for a typical LES result is shown in Figure 1(b). This figure outlines the thermal plume streak structure before the cylinder and the thermal caps noted due to the heated outer cylinder surface.

The experimental configuration was modeled using a RANS/hybrid-RANS approach (Laskowski *et al.* 2007) with varying success. Specifically, when the bottom wall was not heated, the heat flux predictions were adequate. Otherwise, when the bottom wall was heated, the ability to obtain accurate QoI predictions in heat flux were significantly challenged. For example, heat flux at the stagnation point (case 4) was overpredicted by approximately 150%. In fact, the study clearly demonstrated that the inclusion of turbulent plume structures due to the heated bottom wall surpassed the RANS ability to capture this complex physics, and therefore failed to properly capture the incoming thermal boundary layer. This reduced-mixing prediction resulted in substantially overpredicted heat fluxes at the stagnation point. For more details on the RANS study, the reader is referred to Figure 11 in Laskowski *et al.* (2007).

Although a RANS-based approach was found to be insufficient for the most challenging flow configuration (case 4, in which the Richardson number based on cylinder diameter was 9.3), the successful use of direct numerical simulation (DNS) is noted (Kang *et al.* 2009). In this simulation study, a DNS was performed that yielded good comparisons to the data when an inner conjugate heat transfer approach was used in conjunction with an outer optimization loop for internal heat flux. Recognizing that RANS has been proven to be insufficient for the application space characterized by a buoyant, turbulent low-Mach-number flow and that DNS, although viable for the low-speed heated cylinder case, is not scalable for the $\mathcal{O}(10)$ meter pool fire application, validation of this flow using the LES technique is therefore desired.

2. Low-Mach-number governing equations

The integral form of the Favre-filtered, variable-density continuity equation solved is

$$\int \frac{\partial \bar{\rho}}{\partial t} \mathrm{d}V + \int \bar{\rho} \tilde{u}_j n_j \mathrm{d}S = 0, \tag{2.1}$$

where $\bar{\rho}$ is the filtered fluid density, and $\tilde{u}_j$ is the density-weighted, i.e., Favre-averaged, fluid velocity.

The momentum equation used for LES turbulent transport, also in integral form, is

$$\int \frac{\partial \bar{\rho} \tilde{u}_i}{\partial t} \mathrm{d}V + \int \bar{\rho} \tilde{u}_i \tilde{u}_j n_j \mathrm{d}S = \int \tilde{\sigma}_{ij} n_j \mathrm{d}S - \int \tau_{ij}^{sgs} n_j \mathrm{d}S + \int (\bar{\rho} - \rho_\circ) g_i \mathrm{d}V, \tag{2.2}$$

where $\rho_\circ$ is a reference density, and g is the gravitational acceleration. The subgrid-scale turbulent stress τ_{ij}^{sgs} is defined as

$$\tau_{ij}^{sgs} \equiv \bar{\rho}(\widetilde{u_i u_j} - \tilde{u}_i \tilde{u}_j), \tag{2.3}$$

while the Cauchy stress definition is

$$\sigma_{ij} = 2\mu \tilde{S}_{ij}^* - \bar{P} \delta_{ij}, \tag{2.4}$$

where $\tilde{S}_{ij}^*$ is the traceless rate-of-strain tensor given by

$$\begin{aligned} \tilde{S}_{ij}^* &= \tilde{S}_{ij} - \frac{1}{3} \delta_{ij} \tilde{S}_{kk} \\ &= \tilde{S}_{ij} - \frac{1}{3} \frac{\partial \tilde{u}_k}{\partial x_k} \delta_{ij}. \end{aligned} \tag{2.5}$$

In a low-Mach-number flow, $\bar{P}$ is the perturbation about the thermodynamic pressure, P^{th}. For LES, τ_{ij}^{sgs} represents the subgrid stress tensor and requires closure. The deviatoric part of the subgrid stress tensor is

$$\tau_{ij}^{*sgs} = \tau_{ij}^{sgs} - \frac{1}{3} \delta_{ij} \tau_{kk}^{sgs}, \tag{2.6}$$

where the subgrid turbulent kinetic energy is expressed as $\tau_{kk}^{sgs} = 2\bar{\rho}k$. Here, k represents the modeled turbulent kinetic energy, formally defined as

$$\bar{\rho} k = \frac{1}{2} \bar{\rho} (\widetilde{u_k u_k} - \tilde{u}_k \tilde{u}_k). \tag{2.7}$$

For low-Mach-number flows, a vast majority of the turbulent kinetic energy is contained in the resolved scales. For this reason, the subgrid turbulent kinetic energy is not directly treated but rather is included in the pressure as an additional normal stress. The Favre-filtered momentum equations then become

$$\begin{aligned} &\int \frac{\partial \bar{\rho} \tilde{u}_i}{\partial t} \mathrm{d}V + \int \bar{\rho} \tilde{u}_i \tilde{u}_j n_j \mathrm{d}S + \int p n_i \mathrm{d}S = \\ &\int 2(\mu + \mu_t) \left(\tilde{S}_{ij} - \frac{1}{3} \tilde{S}_{kk} \delta_{ij} \right) n_j \mathrm{d}S + \int (\bar{\rho} - \rho_\circ) g_i \mathrm{d}V, \end{aligned} \tag{2.8}$$

where LES closure models for the subgrid turbulent eddy viscosity μ_t are either the constant coefficient Smagorinsky, WALE or the constant coefficient k_{sgs} model.

The integral form of the low-Mach-number, Favre-filtered static enthalpy energy equation in the absence of species transport used for turbulent transport is

$$\int \frac{\partial \bar{\rho}\tilde{h}}{\partial t}\mathrm{d}V + \int \bar{\rho}\tilde{h}\tilde{u}_j n_j \mathrm{d}S = -\int \bar{q}_j n_j \mathrm{d}S - \int \tau_{h,j}^{sgs} n_j \mathrm{d}S. \tag{2.9}$$

Under general unity Lewis number applications, the diffusive heat flux vector simplifies to $\bar{q}_j = -\mu/\mathrm{Pr}\,\partial\tilde{h}/\partial x_j$, whereas the subgrid-scale turbulent diffusive flux vector τ_h^{sgs} is defined as

$$\tau_{h,j}^{sgs} \equiv \bar{\rho}\left(\widetilde{hu_j} - \tilde{h}\tilde{u}_j\right). \tag{2.10}$$

When using the gradient diffusion hypothesis, the closure is $\tau_{h,j}^{sgs} = -\mu_t/\mathrm{Pr}_t\,\partial\tilde{h}/\partial x_j$.

2.1. *Large-eddy simulation model closure*

In this study, we considered two standard static-coefficient algebraic LES models and one transport-based approach. A dynamic approach exists for each of these models, however, for simplicity were not used herein. The standard Smagorinsky LES closure model approximates the subgrid turbulent eddy viscosity using a mixing length–type model, where the LES grid filter size Δ provides a natural length scale. In all cases, the filter scale is directly proportional to the local mesh size. In the interest of space, the formal description of the Smagorinsky and k_{sgs} models used in this study can be found in the the work by Chai & Mahesh (2012), while a description of the WALE model is provided in Nicoud & Ducros (1999).

2.2. *Numerical implementation*

The simulation study used a low-order (P=1) edge- and element-based equal-order interpolation method. Also included in the study is a high-order (P=2) control volume finite element method. This discretization scheme is used in the context of an approximate pressure projection scheme that is order $P + 1$ accurate in space and second-order in time. For more details of the numerical method tested, the reader is referred to Domino (2014) or to the Nalu open-source code base at github (Domino 2015).

3. Code verification

The method of manufactured solutions (MMS) was used to prove the spatial order of accuracy of the underlying numerical method. As noted, the physics of the flow was characterized as a low-Mach-number variable-density flow in which density and property variations are provided by a non-isothermal configuration. A steady, three-dimensional MMS for an ideal gas equation of state with buoyancy used was given by

$$u = -U_o \cos(a\pi x)\sin(a\pi y)\sin(a\pi z) \tag{3.1}$$

$$v = +U_o \sin(a\pi x)\cos(a\pi y)\sin(a\pi z) \tag{3.2}$$

$$w = -U_o \sin(a\pi x)\sin(a\pi y)\cos(a\pi z) \tag{3.3}$$

$$p = -P_o/4(\cos(a_p\pi x) + \cos(a_p\pi y) + \cos(a_p\pi z)) \tag{3.4}$$

$$h = +H_o \cos(a_h\pi x)\cos(a_h\pi y)\cos(a_h\pi z), \tag{3.5}$$

where U_o, P_o and H_o are unity while a, a_p and a_h are 20, 2 and 10, respectively. The simulation was run with an arbitrary gravity vector with a reference density of unity on meshes of uniform refinement. Finally, an ideal gas equation of state was used along with an enthalpy/temperature relationship of constant specific heat. Figure 2 outlines the

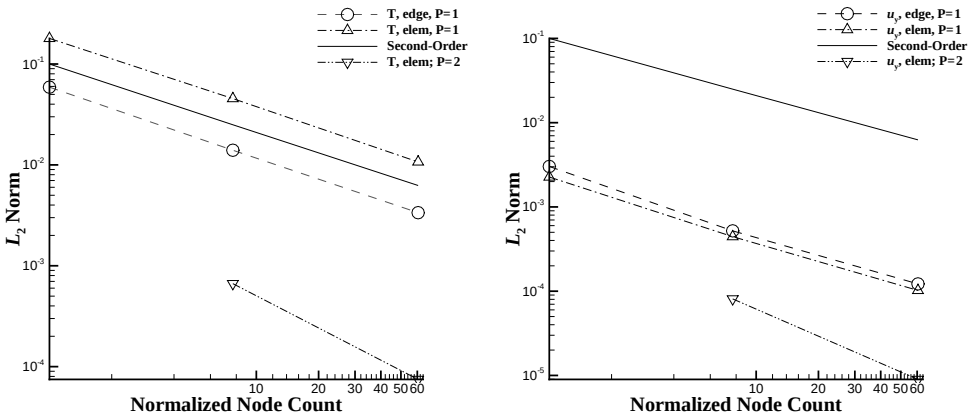

(a) (b)

FIGURE 2. Manufactured solution code verification results (L_2 norm). (a) Temperature order of accuracy. (b) u_y velocity component order of accuracy.

edge-based and element-based steady MMS convergence. Results demonstrated second- and third-order convergence for the P=1 and P=2 schemes in both temperature and velocity L_2 norm (shown only the y-component). It is also worth noting the dramatic reduction (nearly two orders of magnitude) in temperature solution norm.

4. Solution verification

The ability to ascertain convergence of an LES as below is problematic in that both the numerical method and the model are tied to the filter size. Although explicit methods exist, for an unstructured method such filtering operations can be expensive. As such, solution verification was demonstrated via a series of mesh refinement studies.

4.1. *Computational configuration and mesh definition*

All of the simulations within this paper exercised a variable-density, low-Mach-number implementation in which density, viscosity and specific heat properties are solely a function of temperature. Full buoyancy effects were included as per the aforementioned momentum equation, Eq. (2.2).

The unstructured hexahedral coarse mesh (designated refinement zero, or $R0$) was defined by an element count of approximately one million elements and encompassed the entire streamwise facility test section of 61 cm. The simulations used a periodic boundary condition in the spanwise direction. The spanwise width used in this study was found to be sufficiently wide at 10 cm. The subsequent mesh refinements, $R1$ and $R2$, represent uniform refinement steps with adherence to the curvature of the cylinder. Therefore, the element counts for the $R1$ and $R2$ meshes are 8 and 64 million, respectively. The flow configuration for the experimental case 4 are represented by an inflow water velocity of 1.09 cm/s at 284 K. The surface temperature of the cylinder was imposed based on the available experimental data. The values of x^+, y^+, and z^+ for the $R0$ mesh were 2.25, 0.3 and 0.7, respectively. In general, due to the low inflow velocity, from a hydrodynamic

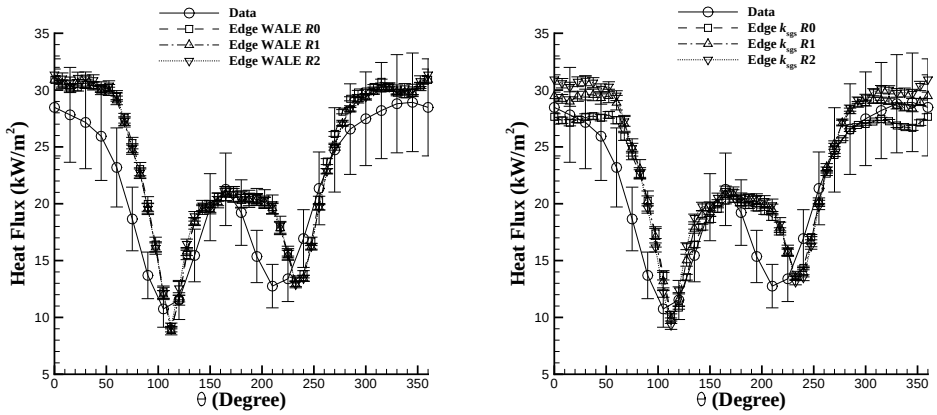

(a) (b)

FIGURE 3. Prediction of heat flux as a function of θ. (a) Solution verification for the edge-based WALE model. (b) Solution verification for the edge-based k_{sgs} model.

perspective this study can be considered a wall-resolved LES. The complexity of the flow is due to the developing thermal boundary layer and complex thermal plume structures.

4.2. *Heat flux comparisons*

In this study, the primary QoI is heat fluxes to the cylinder surface, which are provided at 7.5 degree intervals around the cylinder (Kearney *et al.* 2005). Due to the complex thermal plume structure impinging the spanwise cylinder section (see Figure 1(b)), convergence of the overall simulations required many flow-through times based on the cylinder diameter. The simulations were deemed statistically converged when the mean heat flux along a spanwise line-of-sight was within one percent of the previous time step and the standard deviation in heat flux was lower than three percent. In general, this corresponded to approximately 300 seconds of physical time – or approximately five full facility flow-through times. In all simulations provided, error bars are included in the plots corresponding to the standard deviation of heat flux over the spanwise domain.

Figure 3(a,b) outlines the prediction of heat flux to the outer cylinder for the WALE and k_{sgs} models. Results demonstrate convergence of the three meshes with far superior increased fidelity of the heat flux near the stagnation point compared with RANS results (Laskowski *et al.* 2007). In Figure 4, the edge- and element-based schemes are compared for the lower-order, as well as for the P=1 edge- and P=2 element-based implementations. Results demonstrate a relatively low dependence on the underlying numerical method. This is likely due to the fact that the simulations are both well resolved and that algebraic models, such as WALE or Smagorinsky, include a model-form dependence on a filter size of $\Delta^{4/3}$, while the k_{sgs} model shows a dependence on a filter size of $\Delta^{5/3}$. However, the full effect of higher-order numerics on LES will be further evaluated in future projects.

5. Eigenvalue decompositon

This paper draws upon the systematic model-form eigenvalue perturbation technique, which was first proposed in a RANS context (Emory *et al.* 2013). Later, the method was

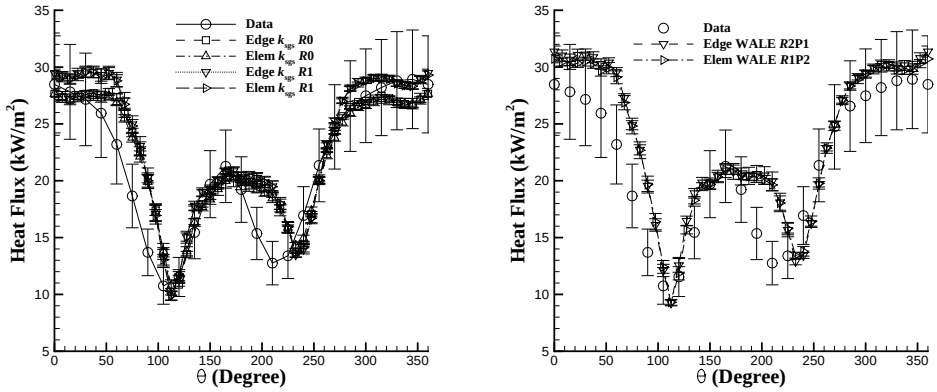

(a) (b)

FIGURE 4. Prediction of heat flux as a function of θ for different numerical implementations. (a) Comparison between the low-order edge- and element-based k_{sgs} model. (b) Comparison between the low-order edge-based WALE model and the higher-order element-based WALE model.

extended to account for scalar transport (Gorle & Iaccarino 2013). This novel technique respresents a systematic way to explore model-form (or structural uncertainty) in turbulence closure models. The technique involves defining a normalized turbulent anisotropic stress of form

$$b_{ij} = \frac{\overline{u_i u_j}}{2k} - \frac{1}{3}\delta_{ij}. \tag{5.1}$$

The above normalized stress tensor can be decomposed into a set of eigenvalues and eigenvectors which result from a simple 3×3 matrix diagonalization. The eigenvectors form a coordinate system of principal component axes which are orthogonal to each other. The eigenvalues of this decomposed system represent the magnitude of the tensor toward the one-, two- and three-component turbulence limiting states. As described in Emory (2014), the barycentric map represents a convenient description of the turbulence state at pointwise locations in the flow. Therefore, model-form uncertainty can be injected into the turbulent stress closure model by perturbation of the 1) turbulent kinetic energy, 2) three directions of the eigenvectors basis and 3) two eigenvalue magnitudes.

Although the above approach can be extended for LES momentum model closures, for scalar SGS closure the gradient diffusion approximation must be extended to allow for a functional form that includes a modeled stress. The generalized gradient diffusion hypothesis (Daly & Harlow 1970) is therefore introduced in an LES context as

$$\tau_{h,j}^{sgs} = -\bar{\rho}\alpha_c \tau_c \tau_{jk}^{sgs} \frac{\partial \tilde{h}}{\partial x_j}, \tag{5.2}$$

where α_c is a model constant ($3/2\, C_\mu/Pr_t$) and τ_c is a time scale (estimated by the inverse rate of strain magnitude). This form, although perhaps not physically justified, allows perturbations to be injected into the scalar SGS closure model. Figure 5(a,b)

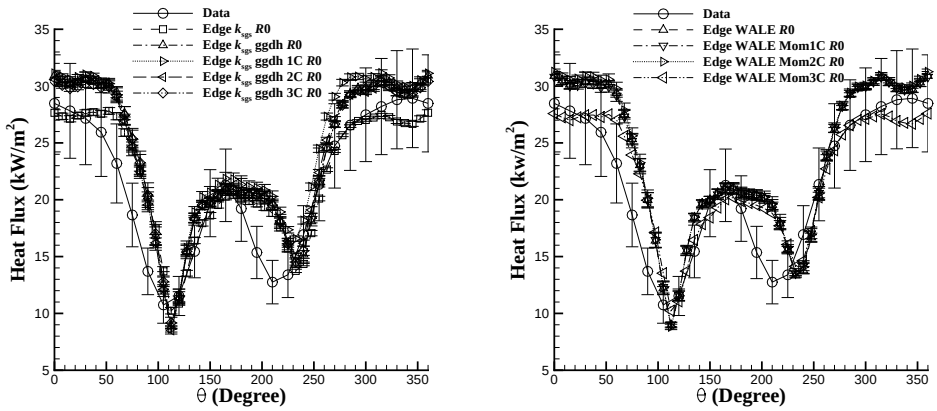

(a) (b)

FIGURE 5. Prediction of heat flux as a function of θ for varying perturbation approaches. (a) The effect of one-, two-, and three-component perturbation of the scalar SGS model. (b) The effect of one-, two-, and three-component perturbation of the momentum SGS model.

outlines the effect of perturbing the eigenvalues of the SGS stress in the context of scalar and momentum transport. These preliminary results indicate that perturbation to the respective limiting turbulence states does allow for a range of predicted QoI. The effect of scalar perturbation is small. However, more fundamental work is required to understand the formality of this method in the LES context, specifically, with respect to the realizablity constraints. Therefore, an extension of this work is planned in partnership with the CTR with an emphasis on LES in plane-channel flow.

6. Conjugate approach with dual-fluid solves

Clearly evident from the set of LES simulations is the convergence of all models toward a common heat flux profile. However, disparities between the simulation and experimental data are noted. Moreover, in every perturbation test case, results approached a converged solution and did not approach the experimentally provided results. In this brief section, a multi-physics approach to modeling this system is provided. Specifically, the external flow physics configuration is the same; however, an additional conjugate stainless steel pipe (inner diameter of 6.35 mm) is now included. Therefore, the formerly specified cylinder heat flux is replaced with a full conjugate heat transfer coupling. Within the inner pipe fluid region resides a non-isothermal interior flow (inlet conditions; water at 327 K) at a Reynolds number of 150k (based on the inner pipe diameter). The numerical coupling of the two fluids (inner pipe and outer cross-flow) and conjugate heat conduction is described elsewhere (Domino *et al.* 2007). In short, an unconditionally stable operator split method between the three physics realms was solved in the context of an outer Picard loop. Although the time scale for the inner pipe was much smaller than the outer cross-flow, a minimum time step was used for all physics which was driven by maintaining a Courant number of unity for the cross-flow fluid and 50 for the inner fluid.

Figure 6 provides a comparison between a single-fluid, wall-temperature-specified DNS

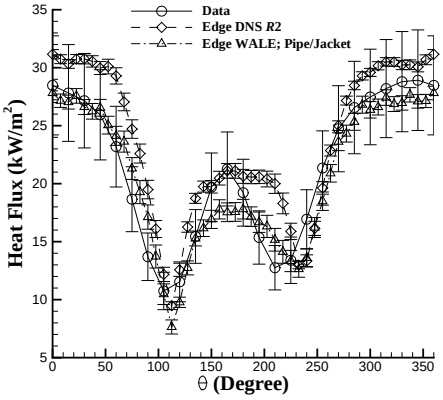

FIGURE 6. Heat flux to cylinder comparing the standard single-fluid simulation with the multi-physics, two-fluid, conjugate coupling.

(using the finest edge-based P=1 method) and an LES which includes an inner (pipe) fluid, a stainless steel pipe and the standard outer fluid cross-flow. Results indicate an increased ability to predict the heat flux when including the full-physics simulation, which is consistent with the previous inner heat flux optimization approach (Kang *et al.* 2009). Also worth noting is that the effect of additional physics to the simulation study represents the greatest effect on the QoI.

7. Conclusions

In this brief, a full validation hierarchy has been outlined which includes problem specification, code verification, solution verification, advanced model-form eigenvalue perturbation techniques and full multi-physics simulations. In order to ascertain model-form sensitivities, formal code verification was demonstrated using a manufactured solution for a three-dimensional, non-isothermal low-Mach-number variable-density flow. This study proved expected design order of accuracy for the underlying edge- and element-based schemes. Simulation results, within the context of a solution verification methodology, demonstrated an increased fidelity in predicted heat flux to the cylinder using a wall-resolved LES technique compared with former RANS-based approaches. In general, the effect of a numerical scheme on the prediction of the mean heat flux QoI was small when the $R1$ and $R2$ mesh resolutions were used. The effect of eigenvalue perturbation techniques formerly conducted within a RANS-based formulation was extended to LES. This model-form perturbation technique demonstrated a small effect on the predicted mean heat flux for both scalar and momentum SGS closures. However, as this study represents the first application of the model-form perturbation technique, future work will focus on more fundamental LES flows including, for example, plane-channel flow. Finally, it was found that although the LES results were convergent to a QoI prediction, the set of heat fluxes deviated from the experimental results. The addition of a multi-physics coupling including an inner flow, outer cross-flow and two-way conjugate coupling demonstrated an increased prediction fidelity of the QoI.

Acknowledgments

Sandia National Laboratories is a multi-program laboratory managed and operated by the Sandia Corporation, a wholly owned subsidiary of the Lockheed Martin Corporation, for the U.S. Department of Energy's National Nuclear Security Administration under contract DE-AC04-94AL85000. SAND2016-10769J.

REFERENCES

Chai, X. & Mahesh, K. 2012 Dynamic k-equation model for large-eddy simulation of compressible flows. *J. Fluid Mech.* **699**, 385–413.

Daly, B. & Harlow, F. 1970 Transport equations in turbulence. *Phys. Fluids.* **13**, 2634–2649.

Domino, S. P. 2014 A comparison between low-order and higher-order low-Mach discretization approaches. *Proceedings of the Summer Program,* Center for Turbulence Research, Stanford University, pp. 387–396.

Domino, S. P. 2015 *Sierra low-Mach Module Nalu: Theory Manual.* Sandia National Laboratories SAND Series SAND2015-3107W, https://github.com/NaluCFD/NaluDoc.

Domino, S. P., Wagner, G., Luketa-Hanlin, A., Black, A. & Sutherland, J. 2007 Verification for multi-mechanics applications. *AIAA Paper* 2007-1993.

Emory, M. 2014 *Estimating model-form uncertainty in Reynolds-averaged Navier-Stokes closures.* Ph.D. Thesis, Stanford University.

Emory, M., Larsson, J. & Iaccarino, G. 2013 Modeling of structural uncertainties in Reynolds-averaged Navier-Stokes closures. *Phys. Fluids.* **26**, 051702.

Gorle, C. & Iaccarino, G. 2013 A framework for epistemic uncertainty quantification of turbulent scalar flux models for Reynolds-averaged Navier-Stokes simulations. *Phys. Fluids.* **25**, 055105.

Gritzo, L. A., Moya, J. L. & Murray, D. 1997 *Fire characterization and object thermal response for a large flat plate adjacent to a large JP-4 pool fire.* Sandia National Laboratories SAND Series SAND97-0047.

Hanlin, A., Domino, S. P., Figueroa, V. & Romero, V. 2009 *Validation and uncertainty quantification of Fuego simulations of calorimeter heating in a wind-driven hydrocarbon pool fire.* Sandia National Laboratories SAND Series SAND2009-7605.

Kang, S., Iaccarino, G. & Ham, F. 2009 DNS of buoyancy-dominated turbulent flows on a bluff body using the immersed boundary method. *J. Comp. Phys.* **9**, 3189–3208.

Kearney, S., Evans, G. & Grief, R. 2005 Experimental investigation of a cylinder in turbulent thermal convection with an imposed shear flow. *AIAA Paper* 2005-1124.

Laskowski, G., Kearney, S., Evans, G. & Grief, R. 2007 Mixed convection heat transfer to and from a horizontal cylinder in cross-flow with heating from below. *Int. J. Heat Fluid Flow* **28**, 454–468.

Nicoud, F. & Ducros, F. 1999 Subgrid-scale modelling based on the square of the velocity gradient tensor. *Flow Turbul. Combust.* **62**, 183–200.

Tieszen, S. 2001 On the fluid mechanics of fires. *Annu. Rev. Fluid Mech.* **33**, 67–92.